



The Effect of Polymer Solubilizing Side-Chains on Solar Cell Stability

Journal:	<i>Physical Chemistry Chemical Physics</i>
Manuscript ID:	CP-ART-02-2015-001158.R1
Article Type:	Paper
Date Submitted by the Author:	22-Mar-2015
Complete List of Authors:	Morse, Graham; Merck Chemicals, Tournebize, Aurélien; Eberhard-Karls-University, Institute for Physical and Theoretical Chemistry Rivaton, Agnes; ICCF, Chassé, Thomas; University of Tuebingen, Taviot-Guého, Christine; CNRS, UMR 6296, ICCF - Clermont Université, Université Blaise Pascal, BP 10448, F-63000, Blouin, Nicolas; Merck Chemicals, Lozman, Owen; Merck Chemicals Ltd., Tierney, Steven; Merck Chemicals Ltd.,

ARTICLE

The Effect of Polymer Solubilizing Side-Chains on Solar Cell Stability

Cite this: DOI: 10.1039/x0xx00000x

G.E. Morse,^{a*} A. Tournebize,^{b,c} Agnès Rivaton,^b Thomas Chassé,^c Christine Taviot-Gueho,^d Nicolas Blouin,^a Owen R. Lozman,^a and Steven Tierney^aReceived 00th January 2012,
Accepted 00th January 2012

DOI: 10.1039/x0xx00000x

www.rsc.org/

Abstract. The impact of side-chain variations on the photothermal stability of solar cells devices containing poly(benzodithiophene-diketopyrrolopyrrole) polymers are investigated in the absence of oxygen. Four different side-chains of benzodithiophene (BDT) are synthesized and copolymerized with diketopyrrolopyrrole (DPP) by Stille polymerization. The photothermal stability is measured as active layer blends with phenyl-C₆₁-butyric acid methyl ester (PCBM) in encapsulated inverted photovoltaic cell architecture with zinc oxide and PEDOT:PSS as transport layers (ITO/ZnO/Active layer/PEDOT:PSS/Ag). Device degradation is correlated to the morphological behavior of the polymer:blend upon AM1.5 illumination (UV-visible light, 50°C) and have been investigated by AFM, XRD, and UV-Vis. Once exposed to the light and to the temperature the BHJ stability is governed by two processes (i) PCBM crystallization and (ii) PCBM dimerization. Dimerization results in a rapid initial performance decrease followed by a more gradual decrease caused by a slower thermally activated crystallization. Depending on the blend morphology, dictated by the polymer's alkyl chain, the two processes occur to different extents thereby modulating the BHJ stability. Thus, of the polymer side-chains explored, linear alkyl side-chains stabilized the bulk heterojunction most effectively followed by no side-chain, alkoxy and branched side-chains. Lowering the concentration of fullerene in the active layer also reduces the rate of degradation across the polymers tested. This is a result of both the rate of crystallization and dimerization of fullerene being dependent on its concentration and the nature of the polymer side-chains. This approach appears to be a general strategy to increase the polymer:PCBM stability.

1. Introduction

The design of high performance polymer solar cells (PSC) has presented a significant research and development challenge to the field of organic photovoltaics (OPV) for over 10 years. Their design has been towards low bandgap polymers tailored to absorb a broader range of photons from the sun in efforts to improve the power conversion efficiency. The commonly used strategy to achieve these low bandgap polymers is to promote internal charge transfer in alternating co-polymers by combining an electron deficient monomer with an electron rich co-monomer leading to the formation of donor-acceptor polymers.¹⁻⁴ These design rules led to the evolution of high performance polymers with the first examples including Si-PCPDTBT,⁵ and PCDTBT.⁶ Significant development of this approach in literature has led to its rapid advancement with devices exceeding an impressive 8% power conversion efficiency (PCE).⁷⁻¹³ By design, these donor-acceptor polymers contain a conjugated backbone to ensure their properties of merit including their semiconducting nature, high absorption coefficient, and high charge carrier mobility. As a corollary, these large π conjugated planar polymeric materials demonstrate strong π - π intermolecular forces of attraction hindering their solubility. Current state of the art polymer semiconductors based on low bandgap polymers are decorated with a selection of linear and/or branched solubilising side-chains to impart solubility and functionality allowing for their application in inexpensive printed device fabrication techniques.¹⁴ Although the impact of these side-chains on the polymer order, phase separation and electronic properties is well understood for benchmark materials, their impact on photostability is still poorly

understood over a wide range of differing side-chains and in some cases is considered a weak point in photostability.¹⁵⁻¹⁹ The widespread adoption of PSC technology is currently limited by their modest photothermal stability and durability of the final PSC encapsulated devices under operational conditions.²⁰ Understanding the photothermal stability of current state of the art PSCs is therefore of paramount importance.

PSCs are largely applied as a blended bulk heterojunction (BHJ) of two phase separated components; an electron donor (a polymer material) and electron acceptor (a fullerene such as phenyl-C₆₁-butyric acid methyl ester, PCBM) components. In a PSC device, this blend is sandwiched between hole and electron blocking layers and then a pair of electrodes (Figure 1). PSC stability can be analysed at many levels: (i) the inherent photochemical stability of the individual donor and acceptor materials, (ii) the morphological stability of the BHJ, and (iii) the stability of the overall device including the stability of cathode, anode and extraction layers. The photochemical stability of champion polymers have been investigated in the literature, namely MDMO-PPV,²¹ P3HT,²²⁻²⁴ PCDTBT,²⁵ Si-PCPDTBT^{26,27} and PBT7.²⁸ Linking device stability to molecular structure is challenging. It requires a wide range of knowhow and techniques in synthetic chemistry and device fabrication to resolve subtle changes to the active layer on the nanoscale. The thorough investigation on photothermal stability of a series of structurally similar polymers with side-chain variation has not yet been explored in this fashion.

Herein we report on the impact of a wide variety of side-chains on a donor-acceptor polymer system in order to specifically investigate the role of solubilising side-chains on PSC stability. In this study, the investigation will focus on commonly used monomers for the development of polymers for PSC. In recent years PSC containing benzodithiophene (BDT) as a donor and diketopyrrolopyrrole (DPP) as an acceptor have gained in popularity and demonstrated power conversion efficiencies greater than 6%.^{29,30} As a model system, different side-chains of benzodithiophene (BDT) are synthesized and co-polymerized with diketopyrrolopyrrole (DPP) forming four low bandgap poly-BDT-*alt*-DPP (PBDDTPP) polymers. The polymers are subsequently characterized, optimized in inverted PSC devices and their stability assessed under AM1.5 irradiation in absence of oxygen and thermal treatment. A detailed investigation of their ageing during AM1.5 exposure by XRD, AFM, UV-Vis and FTIR combines to form a hypothesis on their degradation mechanism that is used to find routes to manage their operational stability. Within the series the polymer with a linear side-chain was most stable.

2. Experimental

BDT monomers and DPP monomers were synthesized according to literature procedures.^{30-32,35-37} PCBM was obtained from Nano-C Inc. and used as supplied. 2,6-Bis(trimethyltin)-4,8-didodecyloxybenzo[1,2-b;3,4-b]dithiophene was prepared as previously disclosed.³⁸ Devices were fabricated on 13 Ω/\square photolithography structured ITO which were cleaned by subsequent sonication in acetone, isopropanol and water.

Inverted Architecture

The zinc oxide transport layer was formed by spin-coating a solution of zinc acetate dihydrate (Aldrich) in DMSO at 160 g/L at 4000 rpm for 10 seconds followed by a 5 minutes thermal anneal process at 300 °C.³³ The active layer was deposited by blade coating inside a glovebox. On top of the active layer 0.9 mL of PEDOT:PSS Clevios HTL Solar SCA 246-9 (Heraeus) was spread and uniformly coated by spin-coating at 1100 rpm for 130 seconds without an annealing step. The silver top electrode was applied by vacuum deposition at 2×10^{-6} mbar at 1-5 Å/s.

Standard Architecture

1 mL of PEDOT:PSS Clevios Al 4083 was spread and uniformly coated by spin-coating at 1000 rpm for 20 seconds and then 4000 rpm for 120 seconds onto a UV ozone treated ITO substrate. The substrate was then heated to 120 °C in a glovebox for 30 minutes. The active layer was deposited by blade coating inside a glovebox. The top electrode comprising 20 nm of calcium and 100 nm of aluminum was applied by vacuum deposition at 2×10^{-6} mbar and 1-5 Å/s.

Encapsulation and measurement

The devices were subsequently encapsulated with a top glass cover slide containing a 120 μm cavity in the center of the slide. The outer edge of the cover slide was sealed using UV curing epoxy. The devices were exposed to AM1.5 in a Newport 94082A Solar Simulator and data was collected using a Keithley (2400) connected through a Keithley (2750) switch system. Thermal heating of the devices was performed on a hotplate. Thermal measurements of the illumination area were measured using a mercury thermometer recording a temperature of 37 °C. The encapsulated devices surfaces reached elevated temperature of 45 ± 1 °C during illumination measured by a RS 1327K infrared thermometer fitted with a thermocouple. The temperature of the internal cavity was measured using the infrared thermometer to be 47 ± 2 °C however the measurement may not be accurate due to the reflective nature of the

silver/glass surfaces and should be considered a minimum temperature. Thermal experiments were performed at a hotplate set-point of 105 °C. The surface temperature was measured at 50 ± 4 °C at the center of each of the devices throughout the experiment.

Transistor mobility and cyclic voltammetry

Mobility measurements of the polymers were measured in top-gate organic transistor architecture. The polymers were dissolved at 7 mg/mL in 1,2-dichlorobenzene (DCB) and cast hot at 100 °C by spincoating for 15 seconds at 500 rpm and 120 seconds at 1200 rpm. The films were then subsequently annealed at 100 °C for 3 minutes and their saturated hole mobilities were measured. Cyclic voltammograms were recorded using a Princeton Applied Research VersaSTAT 4 potentiostat. Films of the polymers were cast from a concentrated chloroform solution onto a platinum wire working electrode. Voltammograms were recorded in an anhydrous acetonitrile solution containing 0.1 M $\text{NBu}_4^+ \text{BF}_4^-$ electrolyte with a platinum wire counter electrode and 0.1 M Ag/AgNO₃ in acetonitrile reference electrode. The solutions were purged with N₂ gas and referenced to an external ferrocene solution which was also used to calculate the ionization potential (IP) and electron affinity (EA) positions ($E_{\text{orbital}} = -(E_{\text{onset}} + 5.1) \text{ eV}$).³⁴ Gel permeation chromatography (GPC) was performed with an Agilent Technologies PL-GPC 220 eluted at 1 mL/min with 140 °C HPLC grade 1,2,4-trichlorobenzene (Aldrich) through a PLgel 10 μm Mixed-B (300 \times 7.5 mm) GPC column. The polymers were analysed with a refractive index detector calibrated with narrow polystyrene standards. Samples were prepared at a concentration of 1 mg/mL and filtered at 140 °C prior to analysis.

UV-Vis, AFM and FTIR

Films of P1, P2, P4 and P6 blends were cast from solution (5:1 chloroform(CF):DCB formulation (see Table 2)). The films were deposited on glass substrates in order to perform UV-visible spectroscopy, AFM and XRD measurements and on KBr substrates for FTIR spectroscopy. Furthermore, the KBr substrates are particularly interesting to investigate the UV range (200-300 nm) which is the region of PCBM absorption. The samples were encapsulated in tubes sealed under vacuum (10^{-6} mbar) in order to eliminate the presence of oxygen. The films were exposed to light (simulated solar irradiation, Xe lamp, 750 Wm^{-2} [300-800 nm], $\sim 45^\circ\text{C}$) and this degradation was monitored by UV-Vis and FTIR spectroscopy. In order to make sure that the vacuum has no impact on the samples, all of them were preliminary sealed and stored for 24 hours in the dark. The UV-visible and FTIR spectra were recorded before and after encapsulation and we have observed no change in the full spectra for all polymer blends. Infrared spectra were recorded in transmission with a Nicolet 760-FTIR spectrophotometer working with OMNIC software. Spectra were obtained using 32 scan summations and a 4 cm^{-1} resolution. Changes in UV-Vis spectra were followed with a Shimadzu UV-2101PC spectrophotometer equipped with an integrating sphere.

X-ray diffraction

X-ray diffraction analyses were made using a PANalytical X' Pert Pro diffractometer equipped with a X' Celerator detector and a Cu anticathode ($K\alpha_1/K\alpha_2$). The instrument was used in the $\theta-\theta$ reflection mode, fitted with a nickel filter, 0.04 rad Soller slits, 5 mm mask, $1/16^\circ$ fixed divergence slit, and $1/32^\circ$ fixed antiscatter slit. XRD data were measured over a range of $1-40^\circ$ (2θ) with a step size of 0.0167° and a total counting time of about 3 h.

4,8-Bis-[5-(2-ethyl-hexyl)-thiophen-2-yl]-2,6-bis-trimethylstannanyl-benzo[1,2-b;4,5-b']dithiophene:

The monomer was prepared following a published literature procedure.³⁵

1.00 g (1.73 mmol, 1.00 *eq.*) of 4,8-bis-[5-(2-ethyl-hexyl)-thiophen-2-yl]-benzo[1,2-b;4,5-b']dithiophene was added to a dried 20 mL microwave vial with a teflon stirrer bar.

The vial was sealed and vacuum/N₂ cycled 3 times to purge the sealed vial. Subsequently a minimal quantity of anhydrous tetrahydrofuran (4.90 mL) was added at which point the solution was a yellow/brown colour. Next, a 1.6 M solution of *n*-butyllithium (3.24 mL, 5.19 mmol, 3.00 *eq.*) in hexanes was added drop wise at room temperature to the vial causing the twice lithiated species to precipitate from solution. The reaction was stirred at room temperature for 1 hour. Chloro-trimethyl-stannane (1 M in hexanes) (5.53 mL, 5.53 mmol, 3.20 *eq.*) was added drop wise and then stirred at room temperature for 30 minutes. The reaction was precipitated in water and extracted with diethylether. The extract was dried over magnesium sulphate and the solvent was removed by rotary evaporation. The resulting product was a light yellow/brown oil/jelly which slowly crystallized at room temperature. The stannyl monomers were subsequently purified by 8 recrystallizations from *iso*-propanol yielding 1.29 g (83% yield, 99.5% pure by HPLC). ¹H NMR (300 MHz, CDCl₃): 7.68 (s, 2H), 7.32-7.31 (d, 2H), 6.91-6.89 (d, 2H), 2.88-2.86 (d, 4H), 1.71-1.65 (br, 2H), 1.51-1.29 (br, 16H), 1.0-0.87 (br, 12H), 0.39 (s, 18H).

2,6-Bis-trimethylstannanyl-benzo[1,2-b;4,5-b']dithiophene: The monomer was prepared following a published literature procedure.³⁶ 1.00 g (5.26 mmol, 1.00 *eq.*) of benzo[1,2-b;4,5-b']dithiophene was added to a dried 20 mL microwave vial with a teflon stirrer bar. The vial was sealed and vacuum/N₂ cycled 3 times. Subsequently anhydrous tetrahydrofuran (40.0 mL) was added. Next, the solution was cooled to -78 °C and 1.7 M solution of *t*-butyllithium (7.73 mL, 13.2 mmol, 2.50 *eq.*) in pentanes was added dropwise forming a white precipitate from solution. The reaction was stirred at -78 °C for 2 hour. Chloro-trimethyl-stannane (1M in Hexanes) (15.8 mL, 15.8 mmol 3.00 *eq.*) was added dropwise and then stirred at room temperature for 2 hours. The reaction was added to diethyl ether and washed with an aqueous sodium bicarbonate solution and water. The extract was dried over magnesium sulphate and the solvent was removed by rotary evaporation. The resulting product was a white solid at room temperature. The stannyl monomer was subsequently purified recrystallization from acetonitrile yielding 1.87 g (69% yield, 99.5% pure by HPLC). ¹H NMR (300 MHz, CDCl₃): 0.28 - 0.60 (m, 18H), 7.42 (s, 2H), 8.28 (s, 2H).

4,8-Didodecyl-2,6-bis-trimethylstannanyl-benzo[1,2-b;4,5-b']dithiophene: The monomer was prepared following a published literature procedure.³⁷ 8.00 g (32.0 mmol, 1.00 *eq.*) of 4,8-Didodecyl-benzo[1,2-b;4,5-b']dithiophene was added to a dried round bottom flask. The flask was sealed and vacuum/N₂ cycled 3 times. Subsequently anhydrous tetrahydrofuran (240 mL) was added. Next, the solution was cooled to -78 °C and 2.5 M solution of *n*-butyllithium (38.3 mL, 95.9 mmol, 3.00 *eq.*) in hexane was added dropwise forming a white precipitate from solution. The reaction was stirred at -78 °C for 30 minutes and then room temperature for 30 minutes. The reaction was cooled back down to -78 °C and chloro-trimethyl-stannane (1M in tetrahydrofuran) (102 mL, 102 mmol, 3.20 *eq.*) was added dropwise and then stirred at room temperature for 1 hour. The reaction was precipitated in water and extracted with diethylether. The extract was dried over sodium sulphate and the solvent was removed by rotary evaporation. The resulting product was a brown oil which slowly crystallized at room temperature. The stannyl monomers were subsequently purified by 8 recrystallizations from *iso*-propanol yielding 9.90 g (76% yield, 99.5% pure by HPLC). ¹H NMR (300 MHz, CDCl₃): 7.50 (s, 2H),

3.25-3.16 (t, 4H), 1.86-1.76 (br, 4H), 1.54-1.23 (br, 36H), 0.93-0.86 (br, 6H), 0.46 (s, 18H).

Polymer synthesis: Each monomer was thoroughly dried in a vacuum oven overnight prior to use. The DPP monomer (0.500 mmol, 1.00 *eq.*) and BDT monomer (0.500 mmol, 1.00 *eq.*) were weighed precisely using a four decimal point balance and added to a dry microwave vial. Fresh tetrakis(triphenylphosphine)palladium(0) (20.3 mg, 0.0200 mmol, 0.0400 *eq.*) was added to the vial which was then sealed and evacuated then purged with nitrogen three times. Degassed toluene (20.0 mL) and dimethylformamide (2.00 mL) were added to the reaction vessel via a syringe and the reaction mixture was then subsequently purged with nitrogen gas for another 15 minutes. The reaction was then placed in a 110 °C oil bath and stirred at 800 rpm until the reaction formed a gel (~ 1 hour). The polymer gels were subsequently precipitated and washed in methanol. The resulting solid polymers were purified by continuous washing via soxlet extraction in acetone, petroleum ethers (40-60), and cyclohexane. The final green polymers were extracted with chloroform by soxhlet, reprecipitated in methanol and collected by filtration. The final polymers were dried overnight under vacuum prior to their characterization.

Polymer P1: 594 mg (99.7% yield).

Polymer P2: 574 mg (99.0% yield).

Polymer P4: 550 mg (94.8% yield).

Polymer P6: 526 mg (87.6% yield).

3. Results

3.1 Monomer and Polymer Synthesis

The BDT monomers were individually synthesized by methods previously outlined in the literature.³⁵⁻³⁷ The subsequent stannyl derivatives were synthesized at high concentration conditions to ensure the precipitation of the dilithiated BDT monomers upon addition of three equivalents of 1.6 M *n*-butyllithium. The dilithiated species were subsequently quenched with trimethyltin chloride resulting in the desired monomers. The DPP monomers were synthesized according to Yang.^{30,39} Polymers (P1-P6) were synthesized by Stille polymerization using standard conditions (Scheme 1, see experimental). The polymerizations proceeded rapidly forming gels at 110 °C in less than 1 hour.

The polymers generally exhibit low solubility and can be generally ordered as P2<P1<P6<P4. Suitable solvents are chloroform (CF), toluene, chlorobenzene, 1,2-dichlorobenzene (oDCB) and 1,2,4-trichlorobenzene. Their low solubility presented challenges for molecular weight characterization by gel permeation chromatography. As a result, the polymers were tested in a GPC operating at 140 °C in 1,2,4-trichlorobenzene. The GPC results conclude that the molecular weights of the polymers range from 32 to 131 kg/mol, a reasonable range for OPV performance,⁴⁰⁻⁴² and in the order of P4<P1<P2<P6 (Table 1). A detailed investigation into the effect of molecular weight, dispersity and trace metal impurities^{42,43} on performance and stability is beyond the scope of this study.

3.2 Properties of the EP polymers and their blends with PCBM

In thin films, the polymer blended with PCBM are green in appearance, absorbing strongly between the ranges of 600-800 nm

with a lambda max of 766, 769, 767 and 777 nm for P1, P2, P4 and P6 respectively (Figure 2). Their absorption onsets are between 800 nm and 900 nm which correlate to an optical band gap of 1.5 eV (Table 1). The frontier orbital energy levels of the pure polymer films were measured by solution cyclic voltammetry. Across the range of polymer side-chains only minimal differences in IP and EA energy levels were observed. The frontier energy levels were measured between -5.3 eV to -5.4 eV for their IP and -3.8 eV to -3.9 eV for their EA and are within the ± 0.1 eV experimental error associated with solution cyclic voltammetry (Table 1).³⁴ The hole mobilities of the polymers were measured in top gate organic transistors. Each of the polymers displayed similar transistor hole mobilities, roughly $0.02 \text{ cm}^2 \text{ V}^{-1} \text{ s}^{-1}$. Overall, the material properties of the polymers in this study are similar in optical absorption, frontier energy levels and hole mobility (Table 2).

3.3 Optimized OPV devices

OPV devices of the polymers blended with PCBM were fabricated in order to investigate their stability. A conventional inverted OPV architecture was used for the devices due to its reported stability in literature - ITO/ZnO/Active layer/PEDOT:PSS/Ag(100nm) (Figure 1).⁴⁴ Each material was optimized by ink formulation, varying solvent selection and concentration. Preliminary screening was performed in oDCB, CF, and a ratio of CF:oDCB. A doctor blade was used to deposit the active layer with a coating speed of 30 mm/s and a blade gap of 0.1 mm. Coatings of P1 and P2 in neat oDCB contained fine undissolved particulate due to the low solubility of the P1 and P2. Coatings were superior from CF, due to their high solubility; however, device performance was generally poor, likely caused by inadequate phase separation. A mixture of CF:oDCB, inspired by the work of Janssen,³⁹ was found to be an ideal solvent/non-solvent mixture resulting in 2-5 minute drying times and sufficient phase separation. A solvent ratio of CF:oDCB was optimized for P1 at a 5:1 ratio for P1:PCBM 1:2 blends. This same solvent formulation was used across the series of polymers to negate the effect of solvents on active layer degradation.

Short circuit current of the devices was optimized by varying concentration in the formulation. The optimal concentrations for P1, P2, P4 and P6 were found to be 12, 10, 20, and 15 mg/mL respectively (Table 2). Once optimized, power conversion efficiencies for the series were all above 2.5% reaching over 5% in the case of P1 (Table 2, Figure 2). These results are well in line with other reports of PBDT-co-DPP polymers in the literature.^{30,31,45} Similar results were obtained when these formulations were tested in a standard device architecture, ITO/PEDOT:PSS/Active layer/Ca(30 nm)/Al(100 nm) (Table 2), albeit with slightly lower performance. The open circuit voltage of the polymer series were between 660 mV and 700 mV which is in good agreement with the model developed by Scharber based on their IP positions.⁴⁶ Despite having similar ionization potentials minor variations in open circuit voltage are observed which we attribute to their difference in sidechains and morphology.⁴⁷ Fill factors across the series were lower in the inverted architecture than in standard architecture which suggests that hole or electron blocking layers in the inverted architecture are causing a space charge effect at the interface. This loss could be mitigated using alternative blocking layers, however substitution was not explored because of the reported device stability of this inverted architecture selected for this study.⁴⁴

Reducing the PCBM ratio to 1:1 led to similar device performance for P2 and P4, with P1 and P6 being significantly lower. The concentrations of the inks were reduced at this ratio to compensate

for the high viscosity produced from increased polymer concentration. Although device performance amongst the polymer series was lower, the results represent unoptimized devices.

3.4 Photodegradation of EP polymers containing films

The evolution of encapsulated films of the polymer/PCBM blends coated on glass and KBr substrates were followed by UV-Vis and FTIR spectroscopy during light exposure (Figure 3, Additional information on pristine absorbance of polymer/blend in Figure S1 and S2). During 100 hours exposure, the polymer region of the UV-Vis spectrum was not impacted for each of the films (Figure 3, 600 – 800 nm region, bottom left). This confirms that the polymers are not photochemically damaged after 100 hours of light exposure ($\sim 45^\circ \text{C}$) or at least the conjugated backbones are unchanged. From FTIR spectroscopy, no significant evolution of the vibrational modes assigned to the polymers was observed confirming that the chemical structure of the polymers are unchanged after 100h of irradiation. However, the PCBM region (200 – 350 nm) was significantly modified. The evolution is given in Figure 3 (bottom right). This behavior has already been observed in many polymer blends exposed to light in inert atmosphere.⁴⁸⁻⁵¹ They attributed this modification to the PCBM dimerization/oligomerization. After 25 hours an important decrease of the ΔAbs is observed for each blend suggesting that the PCBM dimerization is relatively independent of the polymer as Manca et al. have observed (explanation of the ΔAbs measurement is described in Figure S1).⁵⁰ Indeed, the evolution is very similar for P1, P2 and P4, however the PCBM is less impacted when it is mixed with the P6 polymer. Due to similarities of each polymer studied, we believe this change is a result of P6's unique morphology, its propensity to form crystallites and is potentially linked to its polymer physical properties (polymer Mn) and/or the thienyl-ethyl hexyl side chain. The mechanism of dimerization of fullerenes has been studied in the past⁴⁸ and occurs by a photochemical 2+2 cycloaddition when fullerene cages are in close proximity ($\sim 4.2 \text{ \AA}$). In the case of the P6 blend, the miscibility of PCBM within the polymer may be low which would favour crystallite formation over dimerization in the film. FTIR analysis found similar small changes for each of the polymer/PCBM with a decrease of the fullerene skeleton vibrational mode (526 cm^{-1}) due to the 2+2 cycloaddition on the fullerene moieties from dimerization. Crystallization of films can significantly affect FTIR stretches which complicates the interpretation.⁵²

In parallel, topographic images were recorded by AFM (Figure 4). The surfaces of pristine polymer samples are shown in supplementary information (Figure S4). The polymer fullerene blends were smooth with RMS values of 1.1 nm (P1), 1.2 nm (P2), 2.3 nm (P4) and 3.6 nm (P6). The surfaces of P1, P2 and P4 presents a desirable fibrous network similar in appearance to other literature reports of DPP based polymers.⁵³ The P6 surface is very different with the formation of irregular shapes. After 50 hours of light exposure (45°C) we can observe a modification of the surface with the formation of dots (20 – 80 nm diameter) for P1, P2 and P4. The isotropic shapes of the crystallites suggest that the process of their formation is diffusion limited.⁵⁴ The amount of crystallites increases with the ageing time. For P6, we observe the formation of very large blocks homogeneously spread at the surface. In order to have an idea of the very large size of those blocks, the P6 images (50 and 100 hours) are presented at a larger scale ($2 \times 2 \text{ \mu m}$, $Z=20 \text{ nm}$ for P1, P2, P4 and pristine P6 and $10 \times 10 \text{ \mu m}$, $Z=600 \text{ nm}$ for 50 and 100 hours P6). The red squares on the 50 and 100 hours represent the $2 \times 2 \text{ \mu m}$ scale of the other images. These large blocks have a crystalline shape

more visible with the phase mode (See Fig S5) and are attributed to PCBM crystals. This is due to the PCBM diffusion through the polymeric matrix. PCBM crystallization is a thermally induced process that occurs even at relatively low temperature (45 °C)⁵⁵⁻⁶² depending on the thermal stability of the BHJ. From our results, it is clear that the P6 BHJ evolved the fastest. It is then more difficult to assign an order of BHJ evolution between P1 P2 and P4.

As prepared, the polymer blend films display broad 21-25° reflections from alkyl chain packing and π - π stacking (~4 Å). Polymer P4 also displayed additional XRD reflections from the polymer lamella at 4° indicating 22 Å d-spacing. Upon ageing while exposed to AM1.5 illumination in vacuum, structural ordering progressively increased in each of the films. P1, P2 and P4 displayed additional reflections between 2-4° after 100 hours which are commonly associated with inter-chain lamella distances in polymers (Figure 5). An increase in the d-spacing (space between polymer lamella) of polymer P4 upon ageing from 21 Å (0 hours) to 21.5 Å (50 hours) and 22 Å (100 hours) suggests possible PCBM interdigitation as observed in P3HT films.⁶³ At 100 hours the inter-chain lamellas are spaced at 36.8 Å (P1), 19.2 Å (P2), 22.1 Å (P4) while P6 maintains its amorphous appearance. P1 and P6 uniquely displayed a sharp reflection between 25-35°, associated with π - π stacking distances of 2.6 and 3.4 Å respectively. In combination with the AFM analysis, it is possible to conclude that both the surface and the bulk of the polymer/PCBM blends experience an increase in molecular ordering over 100 hours of illumination. Observations of both nanoclusters of PCBM and ordered polymer diffraction confirm the occurrence of the active layer morphological ripening. It is important to note that these measurements were made on films which were confined on a single side (without the physical constraint of the top electrode) which has been identified to reduce the rate of morphological PCBM ripening.⁵⁴ These results should thus be considered as an accelerated test used to identify active layer changes to be expected in a double sided confined device.

3.5 Degradation of EP polymers containing devices

The devices in this study were encapsulated with a glass cover slide and a UV curable epoxy glue. Encapsulation was performed in a nitrogen glovebox to prevent exposure to oxygen because it is known to promote OPV degradation.⁶⁴ The observed degradation of OPV devices in this analysis can be stated to be relatively oxygen free, and that oxygen exposure is not the dominate cause for degradation. This claim is also supported by the similarity in degradation of encapsulated devices to those degraded without encapsulation within a nitrogen filled glovebox (Figure S6).

Our investigation into the degradation of the optimized polymer devices was performed for 110 hours. Upon illumination, the devices reach a surface temperature of 45±2 °C, however, it is likely that the OPV film reaches a higher temperature due to the additional energy absorbed in the light absorbing active layer and the insulating ~200 µm nitrogen filled gap incorporated in the glass cover slide and epoxy encapsulation. The device architecture used in each device was identical. Differences in the stability between the devices can be attributed to differences in the active layer, albeit from potentially many different causes. These causes could include morphological changes, polymer photostability, polymer/blocking layer interactions, polymer/PCBM interactions and migration rates of the electrode materials or blocking layers through the polymer.⁶⁵ Each device was photothermally degraded from an optimized performance starting point thus each device had different starting active layer thicknesses which may impact the analysis. The average combined active area

and interlayer thickness was measured on glass by profilometry to be 120 nm, 120 nm, 330 nm, and 220 nm for P1, P2, P4 and P6 respectively.

Photothermal degradation of the devices progressed differently for each of the active layers. P6 showed a sharp increase in performance in the first two hours of illumination resulting from increased FF and Jsc likely cause by thermal annealing of the active layer leading to improved nanoscale morphology. Each of the polymers displayed a decrease in performance after 25 hours of light soaking. Amongst the four polymers, P2 was shown to be the most stable retaining 80% of its initial PCE after 110 hours of AM1.5 exposure, known as its T_{80} (Table 1). The T_{80} for P6 (37 hours), P1 (23 hours) and P4 (10 hours) were significantly shorter. In terms of degradation rate, in the first 25 hours P2 showed the highest stability. Each of the polymers had reduced degradation rates beyond 25 hours, however relative to their starting PCE, P2 was still the most stable of the series. This initial degradation period, termed “burn-in”, can be caused by PCBM dimerization, morphological changes or by the formation of sub-bandgap states.⁶⁶ In this case the rapid depreciation of the performance can be attributed to the dimerization observed by UV-Vis in these films (Figure 3) which is supported by the detailed work of Distler.⁵¹

Current-voltage analysis during degradation identified different degradation trends. Over the 110 hours there was a minimal change in shunt resistance, however a slow increase in series resistance was noted for each of the polymers (Figure S7). The normalized change in series resistance was nearly identical for P1, P4 and P6, with P2 showing much slower changes. For each polymer the degradation was observed to be dominated by FF and Jsc losses. Each of the devices degraded in FF in a similar fashion, with an initial rapid drop which slows after the first 25 hours. P1 and P2 displays a slow gradual Jsc loss, P2's losses are significantly slower than P1's with only minimal losses in Jsc observed in the 110 hour time-frame. For P4, the Jsc degraded at the same rate as FF. For P6, Jsc dropped rapidly in the first 40 hours followed by a secondary more gradual decrease. P6 uniquely displayed a loss of Voc over the 110 hour experiment. Voc losses commonly indicate a change in nature of blocking layers/active layer interface (interaction, reaction or migration) which could indicate that P6 and PCBM are vertically migrating to opposite electrodes or delamination of the active layer.⁶⁷ This corroborates a theory that the morphology of the active layer is changing during degradation that is further supported by the vertical PCBM cluster formation observed in our AFM investigation in the previous section. Generally, across the polymer series degradation occurs at different rates implying that the nature of the polymer (i.e. variation of the side-chain) itself is directly affecting the rate of PCE loss.

3.6 Controlled morphological ripening

If the rate of degradation of these devices is dependent on the active layer then their degradation can be managed by changing active layer parameters. It is possible that the main source of degradation arises from crystallization or Ostwald ripening in the active layer. Ripening⁶⁸ and precipitation from supersaturation⁶⁹ are known processes which have been shown to occur in OPV devices containing PCBM. It is a process which is dependent on the diffusion of the fullerene derivative through the polymeric matrix and is a thermally activated process.⁵⁶ In the polymer fullerene blends, deposits have been observed to grow with ageing by AFM imaging which is further supported by a progressive increase in film order observed in XRD. The shape of the deposits observed in the

blends by AFM was isotropic, suggesting that the process for their growth is diffusion limited.⁵⁴ If morphological changes are indeed caused by Ostwald ripening of the active layer then it would be expected that (1) the process could be adequately mimicked using an equivalent thermal treatment, and (2) that the process would be dependent on PCBM loading. It is important to note that although temperature is a factor in the crystallite growth it also affects the PCBM diffusion rate, PCBM solubility, and surface tension rendering its relationship to crystal growth complex.

Fresh encapsulated devices were heated at a constant temperature of 50 ± 4 °C, to closely match the temperature during AM1.5 illumination, and performance was measured over 60 hours. The thermal exposure led to similar device degradation to AM1.5 illumination. The rates of degradation for P2, P4 and P6 mimicked the rate of degradation under AM1.5 simulated solar irradiation. The absolute performances of the devices were also similar and within expected batch to batch variation. P1 and P6 displayed a faster rate of degradation upon thermal stress than illumination. This discrepancy may arise from differences in heating uniformity, PCBM dimerization kinetics and/or polymer thermal properties (thermal transition temperatures, crystallization energy or thermal heat capacities). A critical finding was that the trends in thermal degradation of the current-voltage parameters were similar to the trends observed for AM1.5 illumination (Figure 6). These similarities suggest that degradation is strongly associated with thermal morphological changes over these timeframes.

The rate of Ostwald ripening is proportional to the concentration of PCBM. Ergo, reducing PCBM concentration should reduce the rate of morphological change and therefore degradation. To test this hypothesis, devices with a polymer to PCBM ratio of 1:1 were aged under AM1.5 for 110 hours. Across each of the polymers tested, the rate of degradation was reduced significantly (Figure 6; Table 2). The chemical kinetics of the photodimerization of fullerene should also be dependent on its concentration and therefore this process is convoluted.

The T_{80} stability has been improved for all devices for each polymer (Figure 7). Therefore lowering the PCBM concentration may be a general approach to increase the PSC device stability. As we can see with Table 2, this improvement of stability can also reduce the initial performance of the devices. Thus, for P1 and P6, this loss of initial performance is too high to be attractive. However for P2 and P4, a good tradeoff is obtained between efficiency and increasing stability. We can speculate that the charge percolation pathway preserved when reducing PCBM loading which is not likely the case for P1 and P6. It is important to note that once again the current-voltage parameters which lead to the degradation are the same and trends in their degradation match the trends observed for the devices containing a ratio of 1:2 polymer:PCBM. This suggests that although the rate of degradation is reduced, the same failure mechanisms are causing the devices to degrade.

4. Discussion

4.1 Dimerization/crystallization competition.

PCBM dimerization (i) and ripening (ii) have been evidenced from UV-visible spectroscopy and AFM/XRD respectively (Scheme 2). Both of these processes are affected by similar parameters however they are distinct processes.

(i) *Dimerization*: requires a light exposure without oxygen (to avoid triplet state quenching) and a confined fullerene close

proximity (3-4 Å).⁴⁸ The reversibility is possible at temperatures greater than 100 °C.⁵¹ The reaction is dependent on fullerene concentration and diffusion rates (a thermally activated process).

(ii) *Ripening*: is a consequence of the PCBM diffusion and is a purely thermal process. The diffusion strongly depends on the polymer matrix, in other words, the PCBM diffusion is favoured if the polymer chains are relatively mobile at the considered temperature.

In our case, the samples were exposed to light without oxygen and at a temperature below 100 °C. Therefore a competition between dimerization and ripening is expected. The 2+2 cycloaddition between two fullerene moieties leads to the formation of dimers. These dimers are less soluble and larger than PCBM which will physically limit their diffusion in the BHJ. Thus, dimerization and crystallization together impact the device performance. Crystallization drives ultimate device failure, while dimerization can lead to very rapid losses in performance over a short timeframe. Dimerization losses are expected to stabilize after 20-30 hours as shown in Figure 3. The picture is however more complex because PCBM dimers are expected to be less soluble and diffuse more slowly than PCBM in a BHJ, thereby reducing crystallization rates. These convoluted processes are further influenced by the initial morphology dictated by the polymer which complicates interpretation. The dimerization process will thus limit changes in the BHJ over time, albeit with lower mobility and performance.⁵¹ The dimers (and potential trimers and/or oligomers) themselves are present as a collection of isomers and do not possess the needed molecular symmetry to crystallize from the BHJ (Scheme 2).

The nucleation density of small molecules on a 2D surface is inversely proportional to the diffusion rate of the material.⁷⁰ If we assume that the nucleation rate is diffusion limited, it is possible to deduce that the number of nucleation sites formed is inversely proportional to the diffusion rate of PCBM within the polymer matrix. As a qualitative tool it is possible to rank the diffusion processes in P1-P6 by counting the nucleation density of crystallites observed in AFM. This qualitative analysis reveals that the diffusion, D , of fullerene is different within each polymer matrix. The diffusion in P2 is slowest such that $D_{P2} \propto 8D_{P1} \propto 15D_{P6} \propto 16D_{P4}$. By AFM it is also possible to estimate the solubility of fullerene within the polymer matrix at operational conditions. As a first approximation we assume that the surface and bulk are similar and that the crystallites are approximated as circles, allowing us to estimate the mass of fullerene which is excluded from the BHJ over time. By this estimate the most mass is excluded from P6 suggesting that it has a low fullerene solubility/miscibility (C) and the polymers can be roughly estimated that $C_{P6} \propto 2C_{P2} \propto 15C_{P1} \propto 120C_{P4}$.

4.2 Influence of the polymer structure

The rate of ripening and dimerization is dependent on similar physical parameters: PCBM diffusion rate, temperature and PCBM solubility in the polymer. PCBM has been found to diffuse at low temperatures in P3HT, as low as 40-50 °C, and is observed to occur at ~50 °C in P1-P6.⁵⁵⁻⁶² The diffusion rate of PCBM through a polymer has also been previously shown to correlate with alkyl chain length.⁷¹ The diffusion rate of a small molecule within a polymer matrix depends more on the nature of the polymer than its molecular weight. Once above a threshold Mw of 10 kg/mol the polymer Tg and small molecule diffusion constants show little change with a further increase in Mw⁷² which suggests it is a function of the chemical structure of the polymer relating to the nature of the side-chain and rigidity of the backbone.⁷³ The diffusion coefficient of a small molecule within a host matrix below its Tg is

strongly correlated to the fractional volume of the amorphous polymer matrix.⁷⁴ It can thus be expected that the polymer which has the most evenly distributed and ordered side-chains, being lowest in void fraction, would most likely limit diffusion. Additionally, branched side-chains cause steric hindrance in solid films⁷⁵ which increases π - π stacking distances⁷⁶ and in turn increase the void fraction and therefore the PCBM diffusion rate. As a corollary, increasing side-chain order decreases π - π stacking distances; locking in place the polymer chains and reducing the paths in 3-dimensional space for fullerene migration (Scheme 3). Using these general rules, our results can be explained in light of the impact of void fraction on PCBM diffusion (kinetic) and PCBM solubility (thermodynamic).

P2, Linear alkyl-chain: P2 is the most stable polymer with ordered linear side-chains and an even distribution of side-chains along the polymer backbone. The polymer aggregates of P2 are densely packed and have the shortest lamella spacing observed by XRD (once exposed to AM1.5) which is likely to reduce the PCBM diffusion rate. The linear C₁₂ chain is expected to lead to the lowest PCBM miscibility as it displays the lowest solvent solubility of the polymer in the series and excluded a large quantity of crystallites in the AFM images at 50 and 100 hours. These nanocrystals, being small and evenly distributed, should not greatly impact performance.

P1, Linear alkoxy-chain: Alkoxy side-chains can rotate freely around the oxygen molecule which should enhance PCBM solubility over P1 which is reflected in a high solvent solubility. The higher PCBM solubility will cause less mass to precipitate in the film. P1 also shows a large lamella spacing suggesting that the free rotation of the alkoxy chain increases disorder and hinders packing which in turn should increase PCBM diffusion rates.

P4, No side-chain: the lack of side-chain on the BDT core in P4 and larger branched chain on the DPP unit has two effects (i) increased PCBM diffusion due to the voids in the polymer backbone and (ii) increased PCBM solubility caused by potential PCBM interdigitation/void filling. The interdigitation of PCBM can be inferred from the increase in lamella spacing with ageing observed by XRD. The PCBM solubility will be highest in this polymer which is reflected in its high solubility, and therefore nanocrystal formation is expected to be greatly reduced (as seen in AFM). Its high solubility and diffusion make it most prone to dimerization but resilient to crystal formation. P4 shows the slowest rate of decay beyond its initial losses (Table 2).

P6, Branched alkylthienyl-chain: The branched alkylthienyl sidechain with both its twisted thienyl group⁷⁷ and its branched side-chain will sterically hinder solid state packing. The branched chain is however bulky and evenly distributed which should reduce the PCBM solubility (reduced void fraction). In this case, low solubility but high diffusion will lead to rapid and large PCBM crystal formation, which does in turn lead to rapid device failure.

5. Conclusions

A series of four low band-gap polymers of poly(BDT-*alt*-DPP) with differing side chains were synthesized by Stille polymerization. The physical properties of the polymers were similar in absorption, mobility, energy levels, and molecular weights. It was shown that a 5:1 CF:DCB solvent formulation resulted in a balance of solubility and drying time to provide adequate nanoscale phase separation with PCBM when processed by doctor blade. The device PCEs ranged from 5.1% (P1) to 2.2% (P4) in inverted architecture devices with

ZnO and PEDOT:PSS as transport layers. The devices were subsequently exposed to AM1.5 solar irradiation at 50°C and their degradation was monitored over 110 hours. Generally, across the polymer series degradation occurs at different rates, suggesting that the nature of the polymer chemical structure itself is directly affecting the rate of PCE loss. We have shown that this process is strongly linked to active layer morphology changes and PCBM dimerization occurring with time observed by AFM, XRD, and UV-Vis analysis of the blend films. The devices could be further stabilized by decreasing the fullerene content to a 1:1 polymer:PCBM ratio suggesting that the device degradation and PCBM migration is diffusion limited in these films. Furthermore, the device degradation was mimicked by thermal treatment of the films (50°C, no light) indicating that morphological changes largely contribute to the device failure. Amongst the polymer series studied, BDT with a linear dodecyl chain was most stable. We demonstrate that stability of the devices is linked to the fullerene diffusion rate for the series of polymers due to the thermal instability of the polymer/PCBM bulk heterojunctions. Amongst the polymer series it was shown that an even distribution of side-chains, preferably linear alkyl, promoted device stability by reducing PCBM diffusion rates. On the contrary, alkoxy and thienyl-ethylhexyl side-chains increase the PCBM diffusion rates in the BHJ by increasing the rotational freedom and steric hindrance of the side-chains. Removing the side-chain promoted PCBM interdigitation and high diffusion rates in the films. These observations made from the data presented herein, combined with other literature precedence, can be used as rule of thumb for reducing morphology changes over time in polymer:PCBM bulk-heterojunction solar cells.

6. Acknowledgements

This research was funded by the European Union Seventh Framework Program (FP7/2011 under grant agreement ESTABLIS n° 290022) and partially by the Natural Sciences and Engineering Research Council of Canada (GEM).

7. Notes and references

[*] Corresponding-Author: Dr. Graham E. Morse
E-mail: graham.morse@merckgroup.com

a - Merck Chemicals Ltd., Chilworth Technical Centre, University Parkway, SO16 7QD, Southampton, United Kingdom

b - ICCF, Equipe Photochimie, CNRS, UMR 6296, BP 80026, F-63171 Aubière, France

c - Universität Tübingen, Institut für Physikalische und Theoretische Chemie, Auf der Morgenstelle 18, 72076 Tübingen, Germany

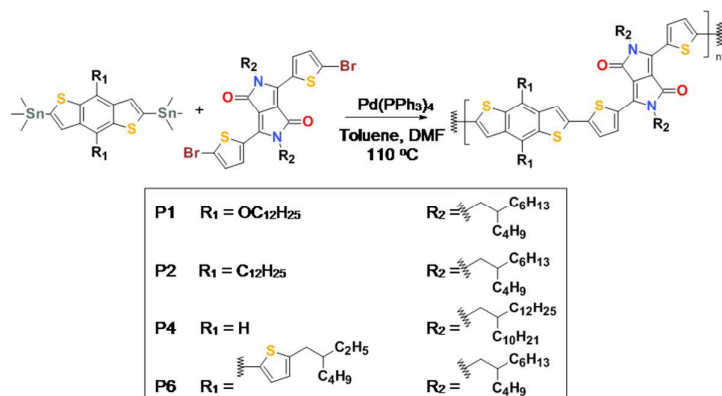
d - ICCF, Equipe Matériaux Inorganiques, CNRS, UMR 6296, BP 80026, F-63171 Aubière, France

Electronic Supplementary Information (ESI) available: including additional UV-Vis, FTIR and AFM images. See DOI: 10.1039/b000000x/

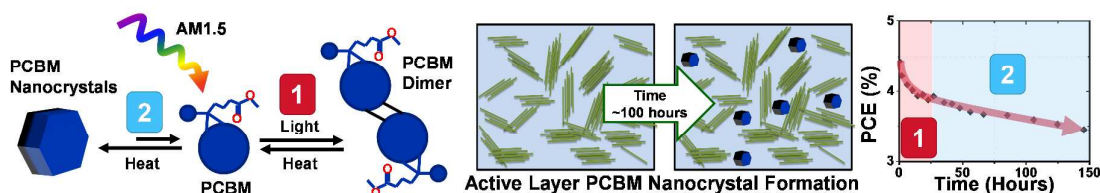
- 1 E.E. Having, W. ten Hoeve, H. Wynberg, *Synth. Met.* **1993**, *55*, 299-306.
- 2 Q. T. Zhang, J. M. Tour *J. Am. Chem. Soc.* **1998**, *120*, 5355-5362.
- 3 H. A. M. van Mullekom, J. A. J. M. Vekemans, E. E. Havinga, E.W. Meijer *Mater. Sci. Eng. R.* **2001**, *32* (1), 1-40.
- 4 A. Ajayaghosh *Chem. Soc. Rev.* **2003**, *32*, 181-191.
- 5 D. Muhlbacher, M. Scharber, M. Morana, Z. Zhu, D. Waller, R. Gaudiana, C. Brabec *Adv. Mater.* **2006**, *18*, 2884–2889.
- 6 N. Blouin, A. Michaud, M. Leclerc, *Adv. Mater.* **2007**, *19*, 2295–2300.
- 7 Z. He, C. Zhong, S. Su, M. Xu, H. Wu, Y. Cao *Nat. Photonics* **2012**, *6*, 593-597.
- 8 X. Li, W.C.H. Choy, L. Huo, F. Xie, W.E.I. Sha, B. Ding, X. Guo, Y. Li, J. Hou, J. You, Y. Yang, *Adv. Mater.* **2012**, *24*, 3046-3052.
- 9 C.E. Small, S. Chen, J. Subbiah, C.M. Amb., S.-W. Tsang, T.-H. Lai, J.R. Reynolds, F. So, *Nat. Photonics* **2011**, *6*, 115-120.
- 10 C. Cabanetos, A. El Labban, J.A. Bartelt, J.D. Douglas, W.R. Mateker, J.M.J. Fréchet, M.D. McGehee, P.M. Beaujuge, *J. Am. Chem. Soc.* **2013**, *135*, 4656-4659.
- 11 T. Yang, M. Wang, C. Duan, X. Hu, L. Huang, J. Peng, F. Huang, X. Gong, *Energy Environ. Sci.* **2012**, *5*, 8208-8214.
- 12 I. Osaka, T. Kakara, N. Takemura, T. Koganezawa, K. Takimiya, *J. Am. Chem. Soc.* **2013**, *135*, 8834-8837.
- 13 J. You, C.-C. Chen, Z. Hong, K. Yoshimura, K. Ohya, R. Xu, S. Ye, J. Gao, G. Li, Y. Yang, *Adv. Mater.* **2013**, *25*, 3973-3978.
- 14 J. Mei, Z. Bao, *Chem. Mater.* **2013**, as soon as publishable, DOI: 10.1021/cm4020805.
- 15 M. Manceau, E. Bundgaard, J.E. Carlé, O. Hagemann, M. Helgesen, R. Søndergaard, M. Jørgensen, F.C. Krebs, *J. Mater. Chem.* **2011**, *21*, 4132–4141.
- 16 L. Liu, S. Tang, M. Liu, Z. Xie, W. Zhang, P. Lu, M. Hanif, Y. Ma, *J. Phys. Chem. B* **2006**, *110*, 13734-13740.
- 17 R. Abbel, M. Wolffs, R.A.A. Bovee, J.L.J. van Dongen, X. Lou, O. Henze, W.J. Feast, E.W. Meijer, A.P.H.J. Schenning *Adv. Mater.* **2009**, *21*, 597–602.
- 18 E. Bundgaard, M. Helgesen, J.E. Carlé, F.C. Krebs, M. Jørgensen *Macromol. Chem. Phys.* **2013**, *214*, 1546–1558.
- 19 A. Rivaton, M. Manceau, S. Chambon, J.-L. Gardette, S. Guillerez, N. Lemaître *Polym. Degrad. Stab.* **2010**, *95*, 278–284.
- 20 M. Jørgensen, K. Norrman, S.A. Gevorgyan, T. Tromholt, B. Andreasen, F.C. Krebs *Adv. Mater.* **2012**, *24*, 580-612.
- 21 S. Chambon, A. Rivaton, J.-L. Gardette, M. Firon, *Sol. Energy Mater. Solar Cells* **2008**, *92* (7), 785-792.
- 22 H. Hintz, C. Sessler, H. Peisert, H.J. Egelhaaf, T. Chassé, *Chem. Mater.* **2012**, *24*, 2739-2743.
- 23 M. Manceau, A. Rivaton, J.-L. Gardette, S. Guillerez, N. Lemaître, *Sol. Eng. Mater. & Sol. Cells* **2011**, *95*, 1315-1325.
- 24 A. Rivaton, M. Manceau, S. Chambon, J.-L. Gardette, S. Guillerez, N. Lemaître, *Polym. Degrad. Stab.* **2010**, *95*, 278–284.
- 25 A. Tournebize, P.-O. Bussiere, P. Wong-Wah-Chung, S. Therias, A. Rivaton, J.-L. Gardette, S. Beaupre, M. Leclerc, *Adv. Energy Mater.* **2012**, *3*, 478-487.

- 26 M. Seck, A. Vincze, A. Satka, D. Hasko, F. Uherek, A. Tournebize, H. Peisert, T. Chasse, *Sol. Eng. Mater. Sol. Cells* **2015**, *132*, 210-214.
- 27 I.F. Dominguez, P.D. Topham, P.-O. Bussière, D. Bégulé, A. Rivaton, *J. Phys. Chem. C* **2015**, *119* (4), 2166–2176.
- 28 S. Alem, S. Wakim, J. Lu, G. Robertson, J. Ding, Y. Tao, *ACS Appl. Mater. Interfaces* **2012**, *4* (6), 2993–2998.
- 29 J.-H. Kim, M. Lee, D.-H. H, *J. Mat. Chem. A* **2014**, *2*, 6348.
- 30 L. Dou, J. Gao, E. Richard, J. You, C.-C. Chen, K.C. Cha, Y. He, G. Li, Y. Yang, *J. Am. Chem. Soc.* **2012**, *134*, 10071–10079.
- 31 J.W. Jung, J.W. Jo, F. Liu, T.P. Russel, H.J. Won, *Chem. Commun.* **2012**, *48*, 6933–6935.
- 32 H. Pan, Y. Li, Y. Wu, P. Liu, B.S. Ong, S. Zhu, G. Xu, *J. Am. Chem. Soc.* **2007**, *129*, 4112-4113.
- 33 M.S. White, D.C. Olson, S.E. Shaheen, N. Kopidakis, D.S. Ginley, *Appl. Phys. Lett.* **2006**, *89*, 143517.
- 34 C.M. Cardona, W. Li, A.E. Kaifer, D. Stockdale, G.C. Bazan, *Adv. Mater.* **2011**, *23*, 2367–2371.
- 35 L. Huo, J. Hou, S. Zhang, H.-Y. Chen, Y. Yang, *Angew. Chem. Int. Ed.* **2010**, *49*, 1500–1503.
- 36 K. Takimiya, Y. Konda, H. Ebata, N. Niihara, T. Otsubo *J. Org. Chem.* **2005**, *70*, 10569-10571.
- 37 Y. Liang, D. Feng, Y. Wu, S.-T. Tsai, G. Li, C. Ray, L. Yu *J. Am. Chem. Soc.* **2009**, *131*, 7792–7799.
- 38 A. Pierre, S. Lu, I.A. Howard, A. Facchetti, A.C. Arias, *J. Appl. Phys.* **2013**, *113*, 154506.
- 39 M.M. Wienk, M. Turbiez, J. Gilot, R.A.J. Janssen, *Adv. Mater.* **2008**, *20*, 2556–2560.
- 40 T.-Y. Chu, J. Lu, S. Beaupre, Y. Zhang, J.-R. Pouliot, J. Zhou, A. Najari, M. Leclerc, Y. Tao, *Adv. Funct. Mater.* **2012**, *22*, 2345–2351.
- 41 C. Muller, E. Wang, L.M. Andersson, K. Tvingstedt, Y. Zhou, M.R. Andersson, O. Inganäs, *Adv. Funct. Mater.* **2010**, *20*, 2124–2131.
- 42 W.R. Mateker, J.D. Douglas, C. Cabanetos, I.T. Sach-Quintana, J.A. Bartelt, E.T. Hoke, A.E. Labban, P.M. Beaujuge, J.M.J. Frechet, M.D. McGehee, *Energy Environ. Sci.* **2013**, *6*, 2529-2537.
- 43 M. P. Nikiforov, B. Lai, W. Chen, S. Chen, R. D. Schaller, J. Strzalka, J. Maser and S. B. Darling, *Energy Environ. Sci.* **2013**, *6*, 1513–1520.
- 44 S.K.H. Hau, H.-L. Yip, N.S. Baek, J. Zhou, K. O'Malley, A.K.-Y. Jen, *Appl. Phys. Lett.* **2008**, *92*, 253301.
- 45 Z. Li, Y. Zhang, S.-W. Tsang, X. Du, J. Zhou, Y. Tao, J. Din, *J. Phys. Chem. C* **2011**, *115*, 18002-18009.
- 46 M.C. Scharber, D. Mühlbacher, M. Koppe, P. Denk, C. Waldauf, A.J. Heeger, C.J. Brabec, *Adv. Mater.* **2006**, *18*, 789–794.
- 47 D.M. Stevens, J.C. Speros, M.A. Hillmyer, C.D. Frisbie, *J. Phys. Chem. C* **2011**, *115*, 20806-20816.
- 48 P.C. Eklund, A.M. Rao, Ping Zhou, Ying Wang, J.M. Holden, *Thin Solid Films* **1995**, *257*, 18S- 203.
- 49 Z. Li, H.C. Wong, Z. Huang, H. Zhong, C.H. Tan, W.C. Tsoi, J.S. Kim, J.R. Durrant, J.T. Cabral, *Nat. Comm.* **2013**, *4*, 2227.
- 50 F. Piersimoni, G. Degutis, S. Bertho, K. Vandewal, D. Spoltore, T. Vangerven, J. Drijkoningen, M.K. Van Bael, A. Hardy, J. D'Haen, W. Maes, D. Vanderzande, M. Nešladek, J. Manca, *J. Polym. Sci. Part B Polym. Phys.* **2013**, *51*, 1209–1214.
- 51 A. Distler, T. Sauermann, H.J. Egelhaaf, S. Rodman, D. Waller, K.-S. Cheon, M. Lee, N. Drolet, D.M. Guldi, *Adv. Energy Mater.* **2014**, *4*, 1300693.
- 52 J.B. Nichols, *J. Appl. Phys.* **1954**, *25*, 840-847.
- 53 W. Li, K.H. Handriks, A. Furlan, W.S.C. Roelofs, M.M. Wienk, R.A.J. Janssen, *J. Am. Chem. Soc.* **2013**, *135* (50), 18942–18948.
- 54 X. Yang, A. Alexeev, M.A. Michels, J. Loos, *Macromolecules* **2005**, *38*, 4289-4295.
- 55 N.D. Treat, M.A. Brady, G. Smith, M.F. Toney, E.J. Kramer, C.J. Hawker, M.L. Chabinyc, *Adv. Energy Mater.* **2011**, *1*, 82–89.
- 56 B. Conings, S. Bertho, K. Vandewal, A. Senes, J. D'Haen, J. Manca, R.A.J. Janssen, *Appl. Phys. Lett.* **2010**, *96*, 163301.

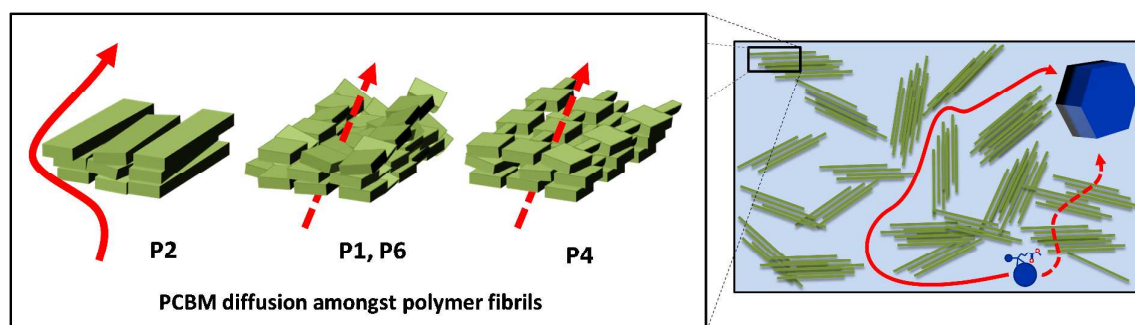
- 57 C. J. Schaffer, C. M. Palumbiny, M. A. Niedermeier, C. Jendrzewski, G. Santoro, S. V. Roth, P. Müller-Buschbaum, *Adv. Mater.* **2013**, *25*, 6760–6764.
- 58 C. Muller, J. Bergqvist, K. Vandewal, K. Tvingstedt, A.S. Anselmo, R. Magnusson, M.I. Alonso, E. Moons, H. Arwin, M. Campoy-Quiles, O. Inganäs, *J. Mater. Chem.*, **2011**, *21*, 10676.
- 59 X. Yang, K.J. van Duren, R.A.J. Janssen, M.A.J. Michels, J. Loos, *Macromolecules* **2004**, *37*, 2151–2158.
- 60 J. Vanderbergh, B. Conings, S. Bertho, J. Kesters, D. Spoltore, S. Esiner, J. Zhao, G. Van Assche, M.M. Wienk, W. Maes, L. Lutsen, B. Van Mele, R.A.J. Janssen, J. Manca, D.J.M. Vanderzande, *Macromolecules* **2011**, *44*, 8470–8478.
- 61 N.D. Treat, T.E. Mates, C.J. Hawker, E.J. Kramer, M.L. Chabinye, *Macromolecules* **2013**, *46*, 1002–1007.
- 62 S. Bertho, G. Janssen, T.J. Cleij, B. Conings, W. Moons, A. Gadisa, J. D’Haen, E. Goovaerts, L. Lutsen, J. Manca, D. Vanderzande, *Sol. Energy Mater. Sol. Cells* **2008**, *92*, 753–760.
- 63 P. Kohn, Z. Rong, K.H. Scherer, A. Sepe, M. Sommer, P. Muller-Buschbaum, R. Friend, U. Steiner, S. Huttner, *Macromolecules* **2013**, *46*, 4002–4013.
- 64 A. Seemann, H.-J. Egelhaaf, C.J. Brabec, J.A. Hauch, *Org. Electron.* **2009**, *10*, 1424–1428.
- 65 M. Jorgensen, K. Norrman, S.A. Gevorgyan, T. Tromholt, B. Andreasen, F.C. Krebs, *Adv. Mater.* **2012**, *24*, 580–612.
- 66 C.H. Peters, I.T. Sachs-Quintana, W.R. Mateker, T. Heumueller, J. Rivnay, R. Noriega, Z.M. Beiley, E.T. Hoke, A. Salleo, M.D. McGehee, *Adv. Func. Mater.* **2012**, *24*, 663–668.
- 67 I.T. Sachs-Quintana, T. Heumuller, W.R. Mateker, D.E. Orozco, R. Cheacharoen, C.J. Brabec, M.D. McGehee, *Adv. Func. Mater.* **2014**, DOI: 10.1002/adfm.201304166.
- 68 S. Kouijzer, J.J. Michels, M. van der Berg, V.S. Gevaerts, M. Turbiez, M.M. Wienk, R.A.J. Janssen, *J. Am. Chem. Soc.* **2013**, *135*, 12057–12067.
- 69 S. Nilsson, A. Bernasik, A. Budkowski, E. Moons, *Macromolecules* **2007**, *40*, 8291–8301.
- 70 R. Ruiz, D. Choudhary, B. Nickel, T. Toccoli, K.-C. Chang, A.C. Mayer, C. Paulette, J.M. Blakely, R.L. Headrick, S. Iannotta, G.G. Malliaras, *Chem. Mater.* **2004**, *16*, 4497–4508.
- 71 L.H. Nguyen, H. Hoppe, T. Erb, S. Gunes, G. Gobsch, N.S. Sariciftci, *Adv. Func. Mater.* **2007**, *17*, 1071–1078.
- 72 T. Cherdhirankorn, V. Harmandaris, A. Juhari, P. Voudouris, G. Fytas, K. Kremer, K. Koynov, *Macromolecules* **2009**, *42*, 4858–4866.
- 73 K. Kunal, C.G. Roberston, S. Pawlus, S.F. Hahn, A.P. Sokolov, *Macromolecules* **2008**, *41*, 7232–7238.
- 74 J.L. Duda, *Pure & Appl. Chem.* **1985**, *57* (11), 1681–1690.
- 75 A.T. Yiu, P.M. Beaujuge, O.P. Lee, C.H. Woo, M.F. Toney, J.M.J. Fréchet, *J. Am. Chem. Soc.* **2012**, *134* (4), 2180–2185.
- 76 Z. Li, S.-W. Tsang, X. Du, L. Scoles, G. Robertson, Y. Zhang, F. Toll, Y. Tao, J. Lu, J. Ding, *Adv. Funct. Mater.* **2011**, *21*, 3331.
- 77 J.-M. Jiang, H.-K. Lin, Y.-C. Lin, H.-C. Chen, S.-C. Lan, C.-K. Chang, K.-H. Wei, *Macromolecules* **2014**, *47* (1), 70–78.



Scheme 1. Chemical structure of polymers P1-P6.



Scheme 2. Illustration of the reaction/mass transport kinetics of PCBM to form PCBM dimers or PCBM nanocrystals. Illumination of the device will cause dimer formation which slows the formation of nanocrystallites. The heat generated by solar irradiation will slowly evolve nanocrystallites during exposure causing ultimate device failure.



Scheme 3. Illustration of different formations of polymer aggregates based on backbone side chain distribution and rotation (left). In the BHJ these aggregates mediate the transport of PCBM which can either pass through the aggregates or around them in a circuitous path (right).

Table 1. Physical properties of polymers P1, P2, P4 and P6.

Polymer	Mn [kg mol ⁻¹] [a]	Mw [kg mol ⁻¹] [a]	PDI [a]	IP (eV) [c]	EA (eV) [c]	Optical gap (eV)	μ_{h-1} [cm ² V ⁻¹ s ⁻¹] [b]
P1	40	130	3.4	-5.3	-3.8	1.5	0.024
P2	93	320	3.5	-5.3	-3.8	1.5	0.023
P4	32	72	2.2	-5.4	-3.9	1.5	0.026
P6	130	730	5.5	-5.4	-3.9	1.5	0.024

[a] Measured at 140 °C in 1,2,4-trichlorobenzene. [b] Saturated hole mobility measured in top gate OTFT deposited from DCB and annealed at 100°C. [c] Approximated by cyclic voltammetry.

Table 2. Device properties of polymers 1-9.

Polymer	Fullerene	D:A ratio	Architecture	Ink conc.	Voc	Jsc	FF (%)	n (%)	T ₈₀ (hr)	Slope in first 24h (%/day)	Slope in last 24h (%/day)
P1	PCBM	1:2	Standard	12	0.64	11.27	60.2	4.35			
	PCBM	1:2	Inverted	12	0.66	15.9	48.9	5.12	22.9	0.904	0.102
	PCBM	1:1	Inverted	10	0.66	8.50	31.2	1.75	60.3	0.289	0.0311
P2	PCBM	1:2	Standard	10	0.71	10.5	57.7	4.26			
	PCBM	1:2	Inverted	10	0.70	12.1	52.4	4.43	110	0.407	0.0729
	PCBM	1:1	Inverted	8	0.72	10.6	46.3	3.52	>110	0.165	0.0340
P4	PCBM	1:2	Standard	20	0.70	5.91	53.9	2.22			
	PCBM	1:2	Inverted	20	0.68	8.75	45.3	2.69	10.4	0.486	0.0598
	PCBM	1:1	Inverted	16	0.70	7.39	43.5	2.25	>110	0.207	0.0116
P6	PCBM	1:2	Standard	15	0.69	8.96	39.4	2.45			
	PCBM	1:2	Inverted	15	0.66	13.6	32.9	2.95	37.4	0.721	0.132
	PCBM	1:1	Inverted	12	0.70	6.26	28.8	1.26	48.9	0.168	0.04153

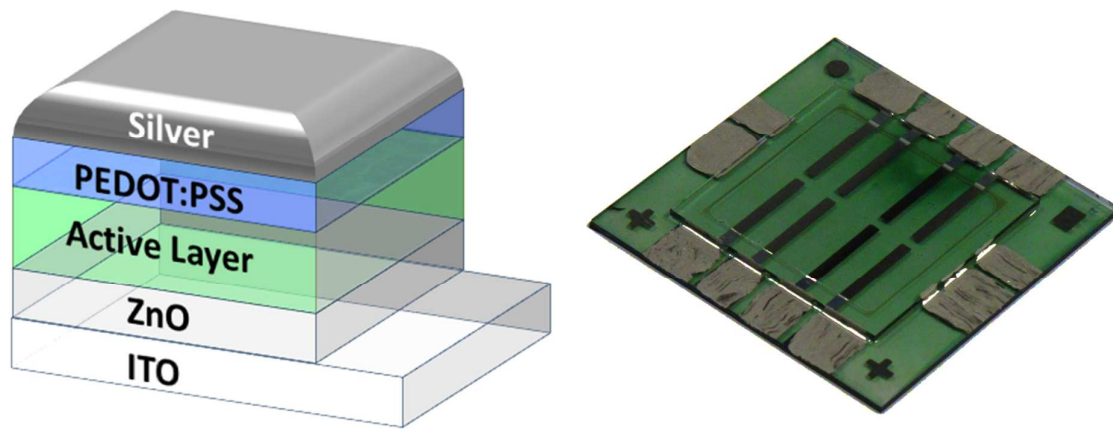


Figure 1. Inverted device architecture (left) and image of final encapsulated device (right).

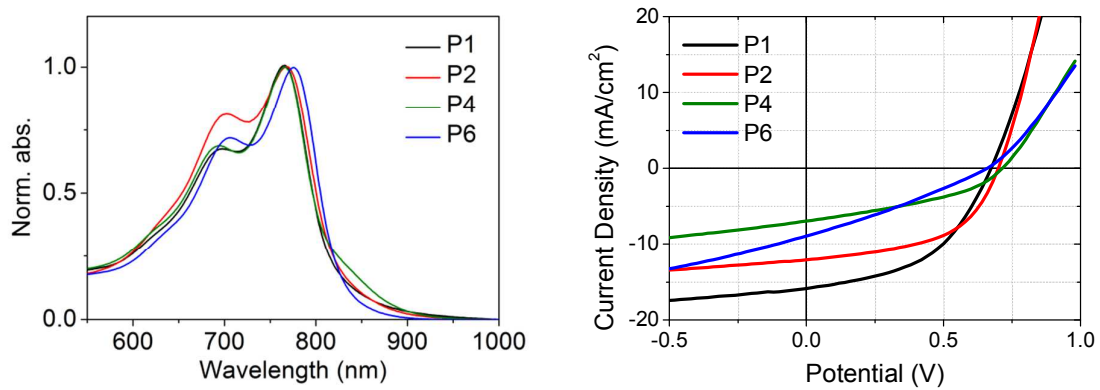


Figure 2. Normalized absorbance in the polymer region of P1, P2, P4 and P6 pristine blends (left) and JV curves of optimized inverted solar cells (right).

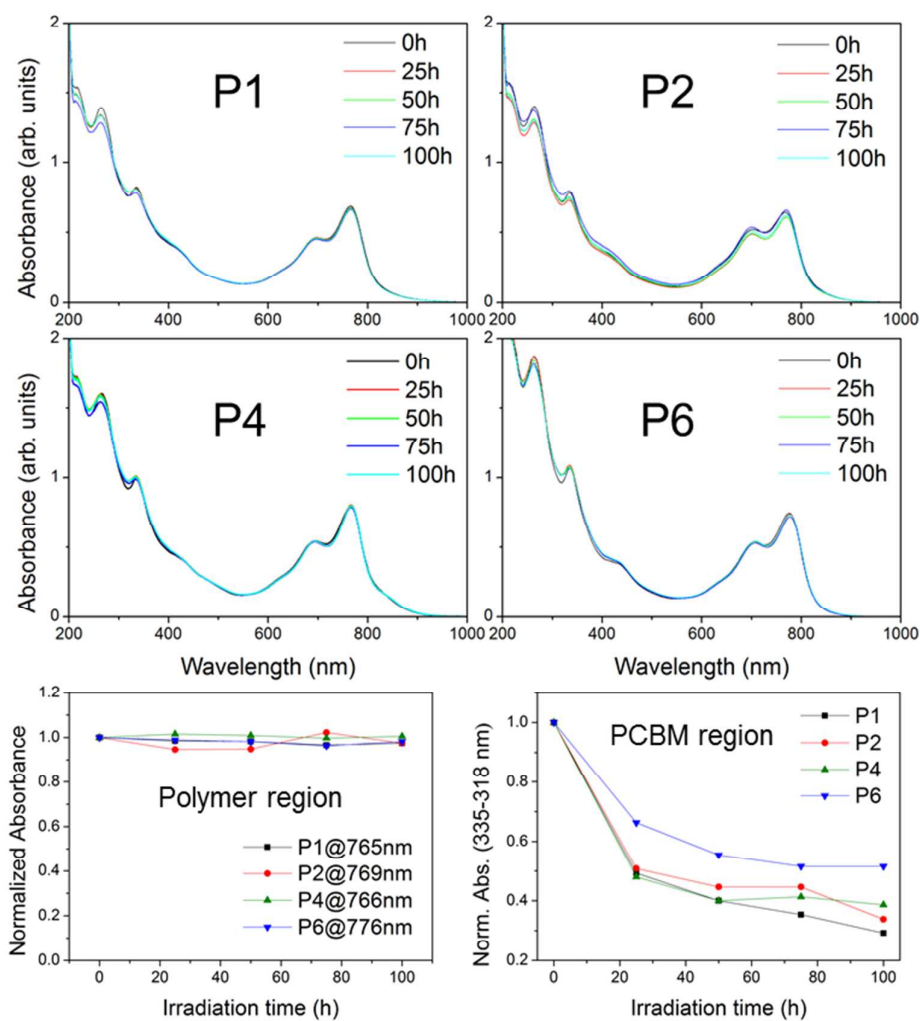


Figure 3. Absorbance changes of the polymer:PCBM (1:2) blends after ageing under AM1.5 simulated solar irradiation. Figures in the bottom left and right show changes in the polymer λ_{\max} and the PCBM 355 nm and 318 nm absorption respectively.

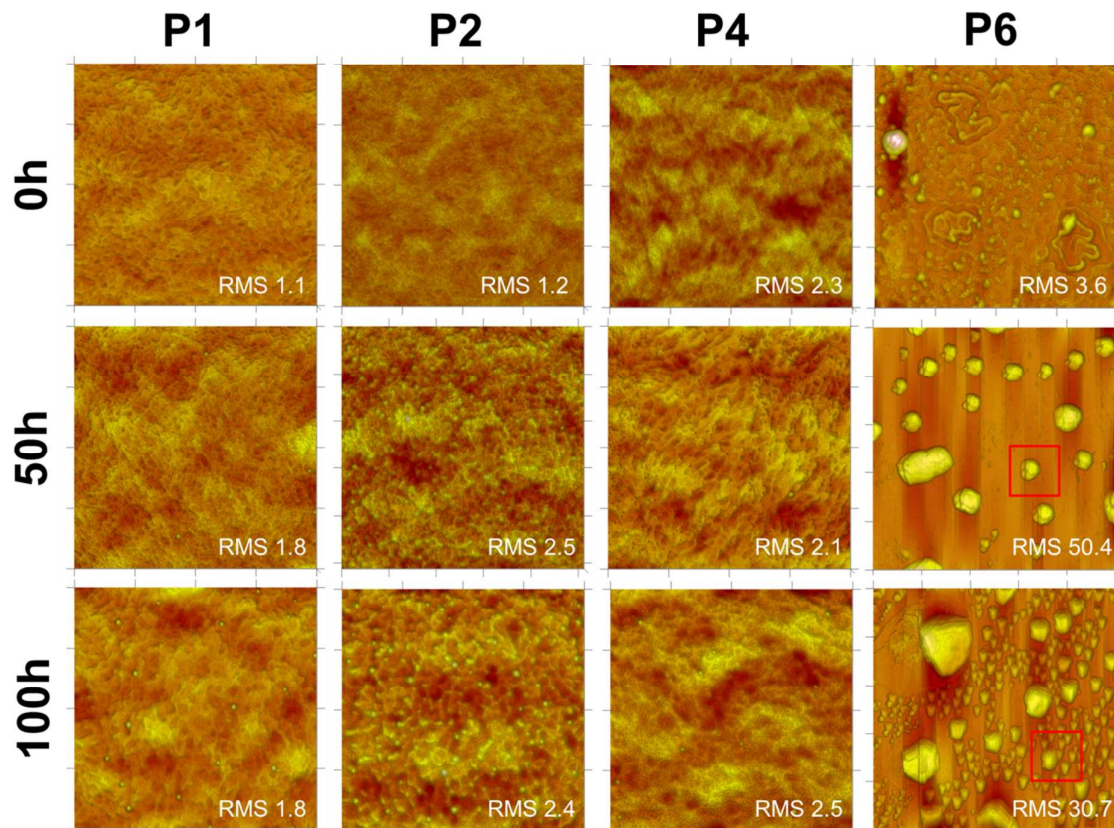


Figure 4. AFM images (Height) of P1, P2, P4 and P6 before (0h) and after 50h and 100h of light exposure at 45°C. The scales are: $X=Y=2\ \mu\text{m}$ and $Z=20\ \text{nm}$ for P1, P2, P4 and pristine P6 images. For P6 50h and 100h, the scale is $X=Y=10\ \mu\text{m}$ and $Z=600\ \text{nm}$. The red squares are $2\times 2\ \mu\text{m}$.

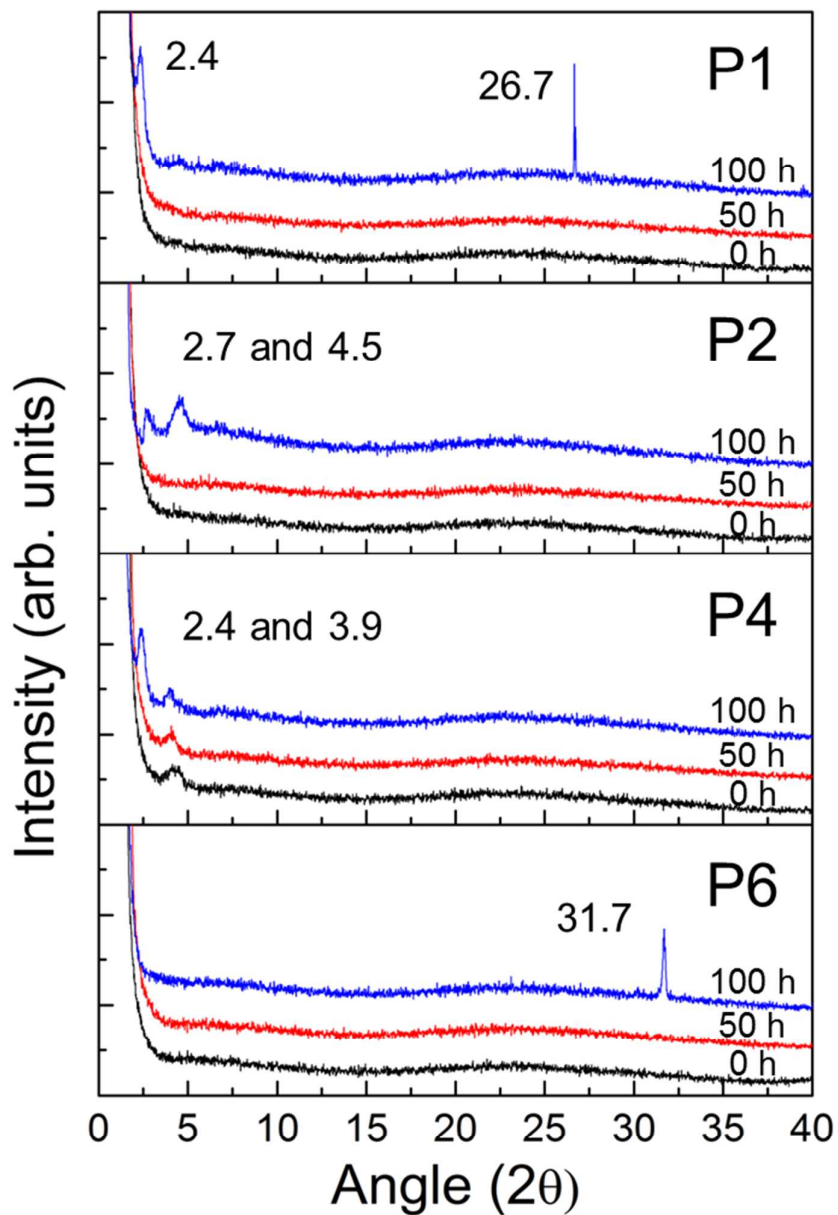


Figure 5. XRD patterns of active layers at different intervals of AM1.5 solar illumination.

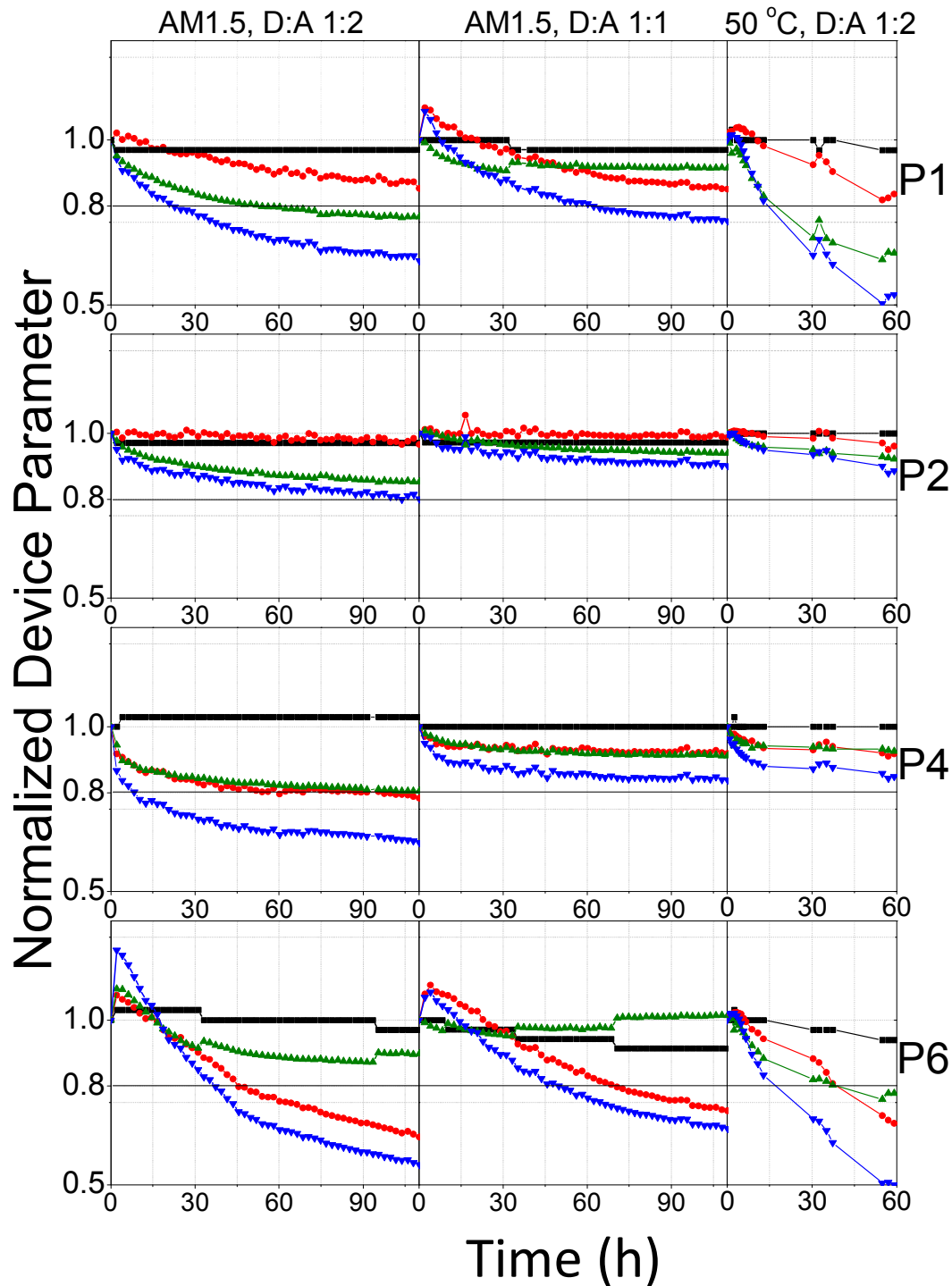


Figure 6. Normalized Jsc (♦), Voc (■), FF (▲) and PCE (▼) degradation of P1-P6/PCBM blends under AM1.5 illumination or thermal exposure.

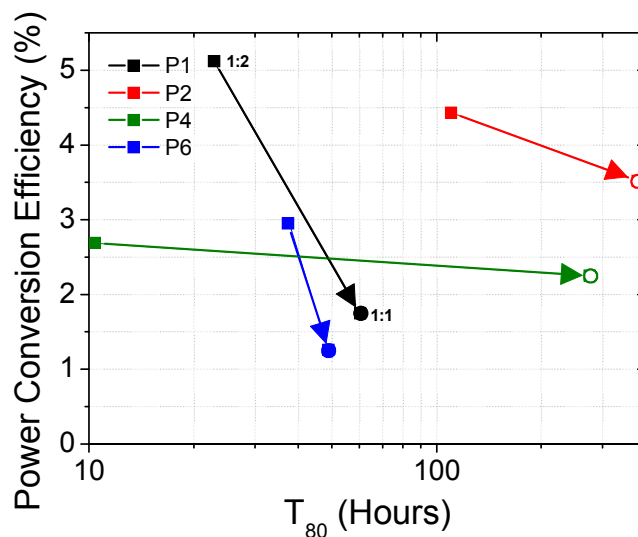


Figure 7. Solar cell power conversion efficiency plotted versus T_{80} (log scale) under AM1.5 illumination for inverted devices containing polymers P1-P6 blended with PCBM. The effect of changing the PCBM loading from 1:2 (square symbol, ■) to 1:1 (circle symbol, ●) polymer:PCBM ratio is visually represented across the series showing a tendency towards more stable devices. A data point with an open circle (○) represents T_{80} estimate by extrapolating the slope observed in the last day of ageing.

The table of contents entry: The impact of polymer side-chains on encapsulated OPV device stability is studied systematically in a series of low bandgap polymers.

Keyword: Photovoltaic Devices, Solar Cells, Fullerenes, Organic Electronics, Photochemistry, Structure-Property Relationships, Conjugated Polymers.

Graham E. Morse,^{a,} Aurélien Tournebize,^{b,c} Agnès Rivaton,^b Thomas Chassé,^c Christine Taviot-Gueho,^d Nicolas Blouin,^a Owen Lozman,^a and Steven Tierney^a*

The Effect of Polymer Solubilizing Side-Chains on Solar Cell Stability

